JVSTA Journal of Vacuum Science & Technology A

Nitriding of AISI 4140 steel by a low energy broad ion source

E. A. Ochoa, C. A. Figueroa, and F. Alvarez

Citation: Journal of Vacuum Science & Technology A **24**, 2113 (2006); doi: 10.1116/1.2356480
View online: http://dx.doi.org/10.1116/1.2356480
View Table of Contents: http://scitation.aip.org/content/avs/journal/jvsta/24/6?ver=pdfcov
Published by the AVS: Science & Technology of Materials, Interfaces, and Processing

Nitriding of AISI 4140 steel by a low energy broad ion source

E. A. Ochoa, C. A. Figueroa, and F. Alvarez[a)]
Instituto de Física "Gleb Wataghin," Universidade Estadual de Campinas (UNICAMP), C.P. 6165, 13083-970 Campinas, São Paolo, Brazil

(Received 15 November 2005; accepted 22 August 2006; published 11 October 2006)

A comprehensive study of the thermochemical nitriding process of steel AISI 4140 by low energy ion implantation (Kaufmann cell) is reported. Different times of implantation were employed and the studied samples were characterized by x-ray diffraction, *in situ* photoemission electron spectroscopy, scanning electron microscopy, and hardness (nanoindentation) measurements. The linear relationship between nitrogen content and hardness was verified. The structure of the nitrided layer was characterized yielding that the compound layer is formed by coarse precipitates, around small grains, constituted principally by ε-$Fe_{2-3}N$ and γ-Fe_4N phases and the diffusion zone is formed by fine precipitates, around big grains of the original martensitic phase, constituted principally by γ-Fe_4N phase. Finally, a diffusion model for multiphase systems was applied to determine effective diffusion coefficients of nitrogen in the different phases. © *2006 American Vacuum Society.* [DOI: 10.1116/1.2356480]

I. INTRODUCTION

The understanding of the diffusion process of light elements such as nitrogen and carbon in iron alloys is of primordial importance since it allows prediction of the nitrogen in depth concentration for different treatment times.[1] Moreover, the mechanical properties of the modified materials by nitriding thermochemical process mostly depend on this concentration profile of element.[2,3] Also, the knowledge of the diffusion process is mandatory to predict the formation of the different crystalline phases forming the modified layer. It is important to note, however, that the microscopic mechanism of the diffusion process in metal alloys is not yet very well understood and the diffusion coefficients in modified multiphase polycrystalline systems are difficult to determine.[4] Last but not the least, due to practical difficulties, few works report experimental correlation between hardness and nitrogen concentration.[5,6]

In this work we report a comprehensive nitriding study of low-alloyed steel (AISI 4140) by low energy nitrogen ion implantation (Kaufmann source) and subsequent thermochemical diffusion. The nitrogen profile in depth and hardness properties are correlated with the observed phase distribution and material microstructure. Finally, a standard multiphase diffusion model was successfully applied allowing effective diffusion coefficients in the nitrided layer to be estimated.

II. EXPERIMENT

Samples 20×10 mm^2 and 1 mm thick, from the same lot of AISI 4140 steel (C%:0.4, Cr%:1.0, Mo%:0.20, Mn%:0.85, Si%:0.25, P%: <0.04, S%: <0.04, Fe:balance), were used for all the studies. The treated samples were mirror polished using standard metallurgical techniques. The material was nitrided by using a low energy ion source (Kaufmann cell)[7] and subsequent thermal diffusion. The implantation chamber (base pressure $<10^{-4}$ Pa) is attached to an UHV x-ray photoemission electron spectroscopy (XPS) system.[8] This experimental set up allows working with a very low oxygen background ($<2\times10^{-5}$ Pa) minimizing unknown parameters which normally complicate the interpretation of the experimental results. The gases were introduced in the ion gun using mass flow-meter controllers and the ions impinge perpendicularly to the surface of the sample. The chamber pressure is monitored using a cold cathode gauge. The ion energy and ion nominal current were fixed at 600 eV and 40 mA, respectively. The process temperature was maintained at 550 °C and the implantation times were 1, 4, and 9 h.

The in-depth profile of the N concentration was performed as follows.[9] After nitriding, the samples were transferred to the XPS chamber for compositional analysis. The nitrogen profile concentration was obtained by repeatedly sputtering and transferring the sample to the UHV XPS measurement chamber.[9] The cleaning procedure was performed at a 0.2 μm/min sputtering rate (1 KeV, Ar^+ beam). This process was repeated several times until a 50 μm depth was reached. Above this thickness, the erosion was performed by *ex situ* 100 μm step mechanical wearing. The sample was then reintroduced in the chamber and a 3 min Ar^+ sputtering cleanup procedure was applied. Therefore, the sample was again transferred into the XPS chamber for N concentration measurements. This procedure was repeated several times until a depth of $\sim$1 mm was reached. It is interesting to note that at $\sim$1 mm depth the hardness is equal to the value at the surface of a virgin sample (3.3 GPa). The phase distribution was studied by x-ray diffraction (XRD) using the Cu $K\alpha$ ($\lambda=1.54$ Å) line, 40 kV, and 30 mA current. In order to analyze the different phases in depth, a progressive and controlled abrasive wear was performed and successive XRD patterns were taken. The cross-section morphology and the thickness of the nitrided layers were measured from scanning electron microscopy (SEM) images (JEOL JMS-5900LV).

a)Author to whom correspondence should be addressed; electronic mail: alvarez@ifi.unicamp.br

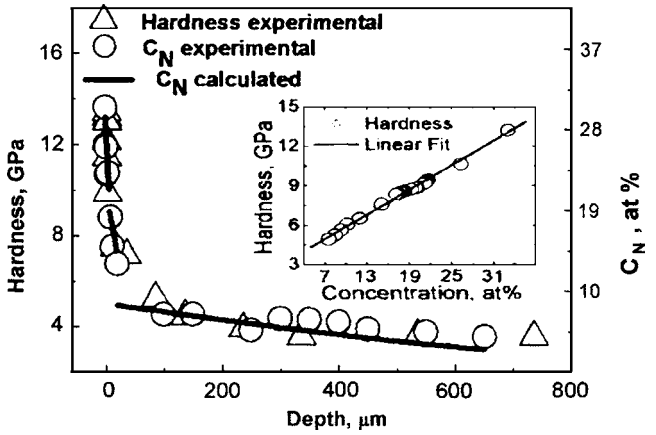

FIG. 1. Nitrogen concentration and hardness profiles of a sample implanted at 550 °C during 9 h. Inset: Linear correlation between both quantities.

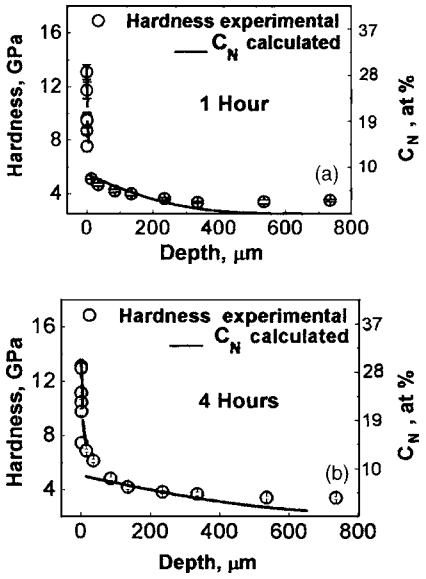

FIG. 2. [(a) and (b)] Nitrogen concentration profiles obtained by using the proportionality coefficient deduced from Fig. 1.

The nitrided layers were revealed, at room temperature, by etching the samples with Nital solution (5 ml of concentrate nitric acid in 194 ml of ethanol). The hardness of samples was measured in cross section, i.e., the samples were sliced perpendicularly to the nitrided surface and mirror polished before indenting measurements. The hardness measurements were performed in a NanoTest 100 apparatus using a Berkovich diamond tip and the results were analyzed using the Oliver and Pharr method.[10] Piling-up effects were not considered. The indentation initial load was ~0.1 mN and the indentation velocity ~3.45 mN s^{-1}. Each reported hardness measurement was obtained averaging five indentation curves. The average standard deviation was around 5%.

III. RESULTS AND DISCUSSION

A. Correlation between hardness and nitrogen concentration in depth

In a previous work, a linear correlation between hardness and nitrogen concentration was established for a system similar to the one studied in this work.[9] What follows is a brief description of the main results obtained in the cited paper. Figure 1 shows the nitrogen profile concentration (right axis) and hardness in depth (left axis) showing the nitrogen concentration versus depth proportionality (inset).

Therefore, hardness versus depth can be converted to nitrogen concentration versus depth by using the proportionality constant obtained from the experimental results (Fig. 1, inset). Figures 2(a) and 2(b) show the converted hardness versus depth curves to nitrogen concentration versus depth for the studied samples.

B. Morphology of the treated samples

Figure 3 shows a sequence of x-ray diffraction patterns corresponding to the 9 h nitrided sample. The patterns were obtained at different depths after successive mechanical erosions of the nitrided layer. The different phases present at variable sample depths are indicated (see Fig. 3, right scale). The surface is principally constituted of ε-$Fe_{2-3}N$. The iron-nitride ε phase has a hcp structure, containing between two and three Fe atoms per unit formula (ε phase: 7.7–9.5 wt % N). Going deeper in the sample, less ε-$Fe_{2-3}N$ and more γ'-Fe_4N nitrides are observed. The iron-nitride γ' phase has a fcc structure, containing four Fe atoms per unit formula (γ' phase: ~6 wt % N). Finally, the γ'-F_4N phase disappears at approximately 100 μm, where the nucleus of α-Fe phase predominates.

Figure 4 shows the microstructure of the sample nitrogen treated during 1 h. From the SEM image, two different zones are identified: (a) the compound layer with smaller grains and coarse precipitates between them, and (b) the diffusion layer with larger grains displaying medium and fine precipitates at the grain boundaries. The interstitial and boundary

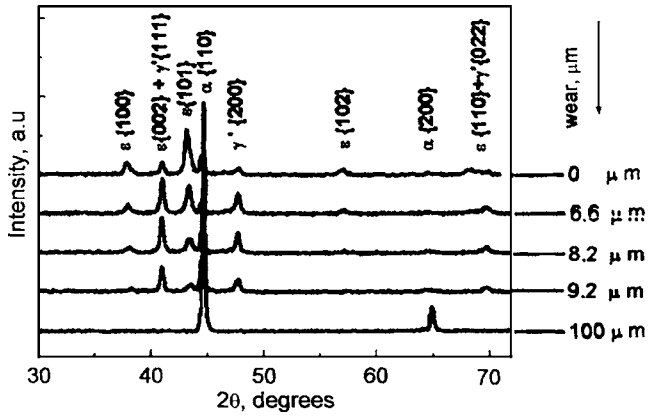

FIG. 3. X-ray diffraction patterns of a sample implanted at 550 °C for 9 h at different depths obtained by a progressive abrasive wear. The right-hand scale represents the depth where the correspondent spectrum was taken.

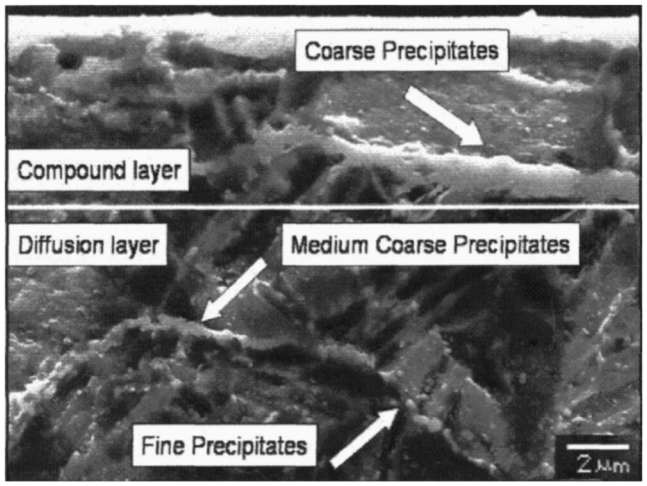

FIG. 4. Cross-section SEM image of a sample implanted at 550 °C and 1 h. The different types of precipitates are indicated.

diffusion paths are the most important mechanisms of nitrogen inclusion in solid metallic solutions. Indeed, nitrogen diffuses faster by grain boundary than by interstitial path.[11] This explains the high concentration of precipitates at the grain boundary observed in the picture (see Fig. 4). Afterwards, nitrogen diffuses from the highly concentrated nitrogen boundaries to the grain bulk. The coarse precipitates are bigger and continuous along the grain boundary. We suggest that they are constituted by a mixture of ε-$Fe_{2-3}N$ and γ'-Fe_4N phases. On the other hand, the fine precipitates are smaller and discontinuous (like small spheres) along the grain boundaries. We suggest that they are constituted by the γ'-Fe_4N phase.

Figure 5 shows quite clearly the interface between the compound and diffusion layers. As revealed by the x-ray spectra, the compound zone is formed by smaller grains and coarse precipitates of ε-$Fe_{2-3}N$ and γ'-F_4N in accordance with the results reported in Ref. 12. On the other hand, the

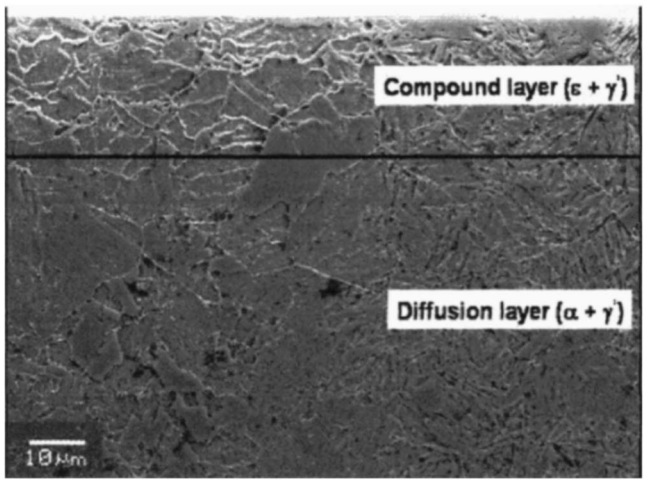

FIG. 5. Cross-section SEM image of a sample implanted at 550 °C and 9 h. The different morphology of the compound and diffusion layers is appreciable.

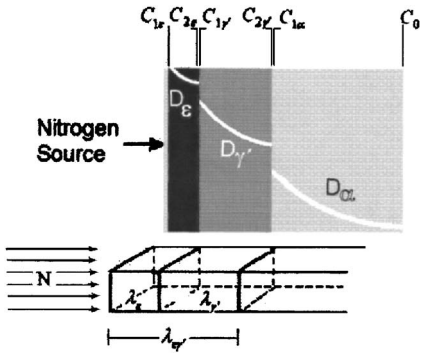

FIG. 6. Parameters and symbols used in the description of the diffusion process of nitrogen. C's and D's represent nitrogen concentration and diffusion coefficient at different interfaces and boundaries, respectively. The boundary coordinates λ's are also indicated.

diffusion zone is formed by larger grains containing a variable nitrogen content (the original martensitic grains) and generally fine precipitates of γ'-F_4N.[13]

C. Nitrogen diffusion process

The classical Fick's laws explain fairly well the nitrogen diffusion process in polycrystalline multiphase systems.[14,15] The model assumes the formation of the different phases in parallel slabs according to the solubility limit of the iron-nitrogen binary system. Moreover, the solid is assumed to be a monocrystalline and the unique diffusion mechanism allowed is the interstitial one. Consequently, the deduced diffusion coefficient represents an effective averaged value since the experimental data are the result of several diffusion mechanisms acting simultaneously. Therefore, the whole volume process determines the kinetics of diffusion. In Sec. III B three zones were identified forming the nitrided layer before reaching the original material nucleus. First, the topmost layer was recognized as ε-FeN_{2-3}; second, an intermediate layer γ'-FeN_4 and, finally, the original nitrogen saturated α-Fe phase containing fine precipitates of γ'-FeN_4 (Fig. 6). Therefore, Fick's law for nitrogen concentration $C_i(x,t)$ in the three regions of interest, namely, ε, γ', and α, is expressed by Eq. (1). Equations (2) and (3) are the corresponding continuity equations at the appropriated interfaces (boundary conditions). In these equations, D_i is the effective

TABLE I. Effective diffusion coefficients at 550 °C for nitrogen in the ε, γ', and α phases. Values from the literature are displayed for the purpose of comparison.

References	$\langle D_N^{(\varepsilon)} \rangle$ ($\mu m^2/s$)	$\langle D_N^{T'} \rangle$ ($\mu m^2/s$)	$\langle D_N^{(\alpha)} \rangle$ ($\mu m^2/s$)
This work	0.06 (+/−0.02)	0.19 (+/−0.02)	6.9 (+/−0.2)
18	0.0246	0.146	7.56
19	0.130	0.081	6.540

diffusion coefficient in the specific regions and λ_i is the coordinate of the time dependent boundary interfaces between layers (Fig. 5).[16,17]

$$\frac{\partial C_i(x,t)}{\partial t} = D_i \frac{\partial^2 C_i(x,t)}{\partial x^2}, \quad i = \varepsilon, \gamma', \alpha, \tag{1}$$

$$(C_{2\varepsilon} - C_{1\gamma'}) \frac{d\lambda_\varepsilon}{dt} = -D_\varepsilon \left.\frac{\partial C_\varepsilon(x,t)}{\partial x}\right|_{x=\lambda_\varepsilon} + D_{\gamma'} \left.\frac{\partial C_{\gamma'}(x,t)}{\partial x}\right|_{x=\lambda_\varepsilon}, \tag{2}$$

$$(C_{2\gamma'} - C_{1\alpha}) \frac{d\lambda_{\varepsilon\gamma'}}{dt} = -D_{\gamma'} \left.\frac{\partial C_{\gamma'}(x,t)}{\partial x}\right|_{x=\lambda_{\varepsilon\gamma'}} + D_\alpha \left.\frac{\partial C_\alpha(x,t)}{\partial x}\right|_{x=\lambda_{\varepsilon\gamma'}}. \tag{3}$$

The diffusion thicknesses of the layers follow a quadratic time law, i.e., $\lambda_\varepsilon = b_\varepsilon \sqrt{t}$ and $\lambda_{\varepsilon\gamma'} = b_{\varepsilon\gamma'} \sqrt{t}$, where b_ε and $b_{\varepsilon\gamma'}$ are constants and t is the process time. The solutions of these sets of equations are resolved in detail elsewhere, giving[16,17]

$$C_\varepsilon(x,t) = A_\varepsilon + B_\varepsilon \operatorname{erf}\left(\frac{x}{2\sqrt{D_\varepsilon t}}\right), \quad 0 < x < \lambda_\varepsilon,$$

$$C_{\gamma'}(x,t) = A_{\gamma'} + B_{\gamma'} \operatorname{erf}\left(\frac{x}{2\sqrt{D_{\gamma'} t}}\right), \quad \lambda_\varepsilon < x < \lambda_{\varepsilon\gamma'},$$

$$C_\alpha(x,t) = A_\alpha + B_\alpha \operatorname{erf}\left(\frac{x}{2\sqrt{D_\alpha t}}\right), \quad \lambda_{\varepsilon\gamma'} < x.$$

From Figs. 1 and 5, the thicknesses of the different nitrided layers for the sample treated during 9 h are estimated ($\lambda_\varepsilon \cong 7\ \mu$m, $\lambda_{\varepsilon\gamma'} \cong 20\ \mu$m). The experimentally determined nitrogen concentration profile is indicated at the right axis of Fig. 1. This information is then employed to numerically resolve the set of Eqs. (1)–(3), allowing the determining of the unknown constants $b_\varepsilon = 0.039\ \mu\text{m s}^{-1/2}$, $b_{\varepsilon\gamma'} = 0.11\ \mu\text{m s}^{-1/2}$, $\langle \mathbf{D}_\text{N}^{(\varepsilon)} \rangle = 0.06(\pm 0.01)$, $\langle \mathbf{D}_\text{N}^{(\gamma')} \rangle = 0.19(\pm 0.01)$, and $\langle \mathbf{D}_\text{N}^{(\alpha)} \rangle = 6.9(\pm 0.2)$. The $\langle\ \rangle$ symbols stand for "effective" diffusion coefficient and we should remember that these values correspond to 550 °C, i.e., the temperature used in the study. Afterward, these constants are used again to numerically resolve Eqs. (1)–(3) for samples treated at different times. The numerical results obtained by applying this procedure are indicated in Fig. 2 (solid lines). A summary of these results is displayed in Table I. Results published in the literature are displayed for the purpose of comparison.

Although Torchane *et al.*[18] and Dimitrov *et al.*[19] did not report experimental errors, the diffusion coefficients determined by these authors are shown in Table I for the purpose of comparison. The larger relative error in the $\langle \mathbf{D}_\text{N}^{(\varepsilon)} \rangle$ determination stems from the fact that the ε thickness, being very thin, is difficult to determine accurately.

IV. CONCLUSIONS

The thermochemical diffusion process of nitrogen in low-alloyed steel AISI 4140 implanted by ion beam was studied. The phase distribution, thicknesses, morphology, and composition of the cross section of nitrided samples were identified by SEM, XRD, XPS, and hardness profile. The nitrogen concentration versus hardness profile proportionality was used to determine the nitrogen profile in nitrided samples at different treatment times. The compound layer is formed by coarse precipitates, around small grains, constituted principally by ε-$Fe_{2-3}N$ and γ'-Fe_4N phases. On the other hand, the diffusion zone is formed by fine precipitates embracing larger grains of the original martensitic phase, constituted principally by the γ'-Fe_4N phase. Assuming Fick's law for a diffusion process in a multiphase system, the nitrogen effective diffusion coefficient in the ε, γ', and α phases were determined.

ACKNOWLEDGMENTS

This work is part of the requirements for the M.Sc. Degree in Physics of one of the authors (E.A.O). The authors are grateful to D. Ugarte and M. Bica for assisting with some measurements and to D. Wisnivesky for helping in the preparation of some samples and discussions. This work was partially sponsored by FAPESP. The SEM measurements were performed at the LNLS. Two of the authors (E.A.O. and C.A.F.) are FAPESP fellows. Another author (F.A.) is a CNPq fellow.

[1] Y. Sun and T. Bell, Heat Treat. Met. **2**, 43 (1997).
[2] L. Trabzon and M. C. Igdil, Surf. Coat. Technol. **200**, 4195 (2006).
[3] S. Mandl and B. Rauschenbach, Defect Diffus. Forum **188–1**, 125 (2001).
[4] Y. Sun and T. Bell, Mater. Sci. Eng., A **224**, 33 (1997).
[5] L. H. Corredor, B. Chornik, and K. Ishizaki, Scr. Metall. **15**, 195 (1981).
[6] I. Alphonsa, A. Chainami, P. M. Raole, B. Ganguli, and P. I. John, Surf. Coat. Technol. **263**, 146 (2002).
[7] H. R. Kaufmann, J. Vac. Sci. Technol. **15**, 272 (1978).
[8] P. Hammer, N. M. Victoria, and F. Alvarez, J. Vac. Sci. Technol. A **16**, 2491 (1998).
[9] E. A. Ochoa, C. A. Figueroa, and F. Alvarez, Surf. Coat. Technol. **200**, 2165 (2004).
[10] W. C. Oliver and G. M. Pharr, J. Mater. Res. **7**, 1564 (1992).
[11] I. Kaur, Y. Mishin, and W. Gust, *Fundamentals of Grain and Interphase Boundary Diffusion*, 3rd ed. (Wiley, Chichester, 1995).
[12] O. Salas, U. Figueroa, J. L. Bernal, and J. Oseguera, Surf. Coat. Technol. **163–164**, 339 (2003).
[13] L. C. Gontijo, R. Machado, E. J. Miola, L. C. Casteletti, and P. A. P. Nascente, Surf. Coat. Technol. **183**, 10 (2004).
[14] F. Dyment, R. H. Tendler, and A. Marajofsky, *Defectos y Difusión en Metales, Compuestos Iónicos y Óxidos*, Reimpresión de la Publicación PMM/A-261 (CNEA, Buenos Aires, 1982).
[15] B. S. Bokshtein, *Difusión en Metales* (Editorial MIR, Moscú, 1980).
[16] P. G. Shewmom, *Diffusion in Solid* (McGraw-Hill, New York, 1963).
[17] J. Crank, *The Mathematics of Diffusion* (Clarendon, Oxford, 1975).
[18] L. Torchane, P. Bilger, J. Duley, and M. Gantois, Metall. Mater. Trans. A **27**, 1823 (1996).
[19] V. I. Dimitrov, G. Knuyt, L. M. Stals, J. D. Haen, and C. Quaeyhaegens, Appl. Phys. A **67**, 183 (1998).